
Physicochemically Informed Dual-Conditioned Generative Model of T-Cell Receptor Variable Regions for Cellular Therapy

Jiahao Ma¹ Hongzong Li² Ye-Fan Hu^{3*} Jian-Dong Huang^{1*}

1: The University of Hong Kong, Hong Kong

2: The Hong Kong University of Science and Technology, Hong Kong

3: BayVax Biotech Limited, Hong Kong

jiahao.ma@connect.hku.hk, lihongzong@ust.hk

yefan.hu@bayvaxbio.com, jdhuang@hku.hk

Abstract

Physicochemically informed biological sequence generation has the potential to accelerate computer-aided cellular therapy, yet current models fail to *jointly* ensure novelty, diversity, and biophysical plausibility when designing variable regions of T-cell receptors (TCRs). We present **PhysicoGPTCR**, a large generative protein Transformer that is *dual-conditioned* on peptide and HLA context and trained to autoregressively synthesise TCR sequences while embedding residue-level physicochemical descriptors. The model is optimised on curated TCR–peptide–HLA triples with a maximum-likelihood objective and compared against ANN, GPTCR, LSTM, and VAE baselines. Across multiple neoantigen benchmarks, PhysicoGPTCR substantially improves edit-distance, similarity, and longest-common-subsequence scores, while populating a broader region of sequence space. Blind *in-silico* docking and structural modelling further reveal a higher proportion of binding-competent clones than the strongest baseline, validating the benefit of explicit context conditioning and physicochemical awareness. Experimental results demonstrate that dual-conditioned, physics-grounded generative modelling enables end-to-end design of functional TCR candidates, reducing the discovery timeline from months to minutes without sacrificing wet-lab verifiability.

1 Introduction

The clinical promise of T-cell-receptor-engineered therapy (TCR-T) [D’Angelo *et al.*, 2024] rests on the rapid discovery of variable regions that recognise patient-specific peptide–HLA complexes with high affinity and selectivity. Classical wet-lab screening cycles require months of iterative cloning and probe only an infinitesimal fraction of the astronomical search space, with 10^{15} – 10^{61} possible TCR sequences by distinct estimations [Mora and Walczak, 2019].

Recent protein language models have begun to reshape macromolecular design: Transformer-based generators [Meier *et al.*, 2021; Ferruz *et al.*, 2022] can now hallucinate enzyme folds and antibodies *in silico*. Yet no prior study has shown that such models can *directly* create biophysically feasible TCR sequences that remain usable in downstream TCR-T pipelines. Compared with antibody or minibinder design (Figure 1A), TCR generation is harder: binding specificity is jointly determined by the presented peptide *and* the polymorphic HLA molecule, and subtle long-range physicochemical couplings often decide success or failure.

*Corresponding author.

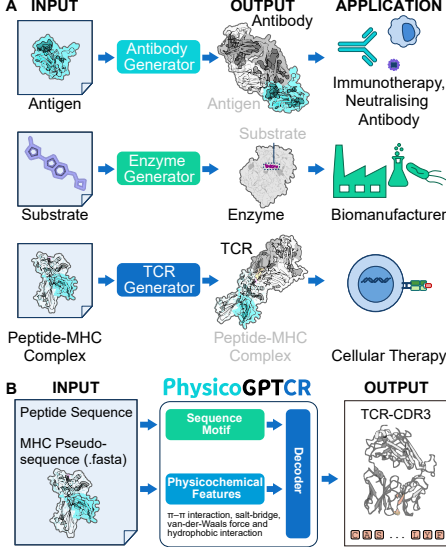


Figure 1: Tasks similar to TCR generation and the workflow. (A) Protein generation analogies. Antibodies can be generated based on antigen inputs, applied to immunotherapy or neutralizing antibodies. Enzymes can be generated for distinct substrates to improve bio-manufacturer. TCR generation is similar to previous two tasks. By requiring peptide-MHC inputs, TCR can be generated for cellular therapies. (B) PhysicoGPTCR workflow: the model processes peptide sequences and MHC pseudo-sequences as inputs, leveraging sequence motifs and physicochemical features through PhysicoGPTCR, followed by a decoder that outputs **TCR CDR3** sequences.

Two technical gaps persist. (1) Vanilla autoregressive models tend to overlook non-local chemical interactions, causing mode collapse or implausible motifs. (2) Models that pursue smoother sequence manifolds seldom encode immunological priors and therefore struggle to enrich for true neoantigen specificity. These issues call for an architecture that *explicitly embeds physicochemical knowledge while remaining end-to-end trainable*.

We respond to this need with **PhysicoGPTCR**, a dual-conditioned generative Transformer that takes the context of the peptide and HLA as input and autoregressively synthesizes TCR variable-region sequences (Figure 1B). The encoder and decoder fuse three information channels—token identity, positional index, and residue-level physicochemical descriptors (aromaticity, charge, hydrogen-bond capacity, molecular mass)—through a learnable gating mechanism, enabling the network to reason about long-range chemical bonds during generation. Training is performed on curated TCR–peptide–HLA triples spanning tumour, autoimmune, viral and bacterial antigens drawn from VDJdb, with maximum-likelihood optimisation only; no post-hoc filters are required.

We benchmark PhysicoGPTCR against four competitive baselines (ANN retrieval, GPTCR, LSTM, VAE) on multiple neoantigen test sets. Across edit-distance, sequence-similarity and longest-common-subsequence metrics, our model *substantially* outperforms all alternatives while populating a broader region of sequence space. A dry-lab activation assay based on blind *in-silico* docking further confirms a higher proportion of binding-competent clones, validating the benefit of explicit physicochemical embeddings.

Our contributions are threefold:

- **Method:** we couple dual biological conditioning with residue-aware physicochemical embeddings, unifying language modelling and chemical-bond reasoning in a single Transformer.
- **Performance:** the approach delivers state-of-the-art generative quality across all string-based metrics and markedly enriches functional hits in dry-lab assays.
- **Impact:** minute-scale inference shortens the TCR-discovery timeline from months to minutes, offering an immediately deployable tool for precision immunotherapy.

2 Related Work

HLA-peptide specificity prediction. Early studies cast T-cell recognition as a *discriminative* task. NetTCR-2.0, DeepTCR and TITAN [Montemurro *et al.*, 2021; Sidhom *et al.*, 2021; Weber *et al.*, 2021] use convolutional, recurrent or attention networks to decide whether a query receptor recognises a given HLA-peptide complex. Although AUC scores keep improving, these classifiers are inherently non-generative and cannot propose novel receptors for TCR-T therapy; moreover, they view sequences as mere symbol strings and ignore the residue-residue couplings that ultimately drive binding.

Generative modelling of TCRs. Only a handful of attempts move beyond classification. TES-SAR [Zhang *et al.*, 2021] explore unsupervised reconstruction but focus on receptor repertoires without conditioning on antigen context. More recently, TCRGPT [Lin *et al.*, 2024] autoregressively samples CDR3 loops conditioned *solely* on the target peptide, leaving the HLA allele unaddressed. None of these works evaluates *dry-lab activation rate* via docking or molecular simulation, and therefore their therapeutic utility remains unclear.

Protein sequence generation at large. Transformer language models such as ProGen, ProtGPT2 and ESM-1v [Madani *et al.*, 2020; Ferruz *et al.*, 2022; Meier *et al.*, 2021] demonstrate that pure sequence modelling can create functional enzymes and antibodies. Structure-aware approaches extend this panorama: RFdiffusion [Watson *et al.*, 2023] and Chroma [Singh, 2024] design full-atom backbones directly, while ESM-IF refines inverse folding with iterative hallucination. Yet these generators are trained on broad protein corpora without any immunological signal, offering no mechanism to bias outputs toward HLA-peptide interfaces.

Physicochemical or structural priors. ProteinMPNN, Atom3D and ESM-Fold re-design [Dau-
paras *et al.*, 2022; Hayat *et al.*, 2015; Lin *et al.*, 2023] inject backbone geometry or energy-inspired terms into sequence design; Rosetta-guided pipelines [Liu and Kuhlman, 2006] combine supervised scoring with Monte-Carlo sampling. Such methods improve foldability but assume a pre-existing 3-D structure, rarely available for highly diverse TCR variable regions, and they do not incorporate the dual antigen-HLA conditioning crucial for immunotherapy.

Gap. In summary, prior studies do not *simultaneously* (1) condition on both peptide and HLA context, (2) embed residue-level physicochemical descriptors during generation, and (3) report dry-lab activation against realistic antigen panels. Our work closes this gap and further benchmarks against ANN retrieval, GPTCR, LSTM and VAE baselines, highlighting gains that translate into higher docking-based activation (such as pmtnet or PISTE [Lu *et al.*, 2021; Feng *et al.*, 2024]) without extra filtering.

3 Methodology

Figure 2 summarises **PhysicoGPTCR**. A dual-conditioned encoder digests the HLA molecule and its bound peptide, while a GPT-style decoder autoregressively emits the T-cell-receptor variable-region sequence.

3.1 Problem Formulation

Let $m \in \Sigma^{L_m}$ denote an HLA heavy chain, $p \in \Sigma^{L_p}$ the presented peptide, and $t \in \Sigma^{L_t}$ a receptor variable-region sequence over the 20-letter amino-acid alphabet Σ . The task is to model the conditional distribution

$$p_\theta(t | m, p)$$

such that samples $\tilde{t} \sim p_\theta$ are syntactically valid, biophysically plausible and strongly biased towards recognising the given HLA-peptide complex.

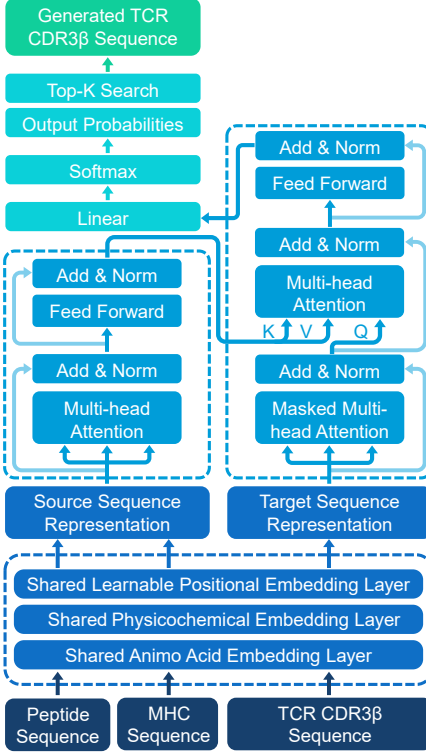


Figure 2: Model overview. Three information channels—token identity, positional index and residue-level physicochemical descriptors—are fused by a gated projector and fed into a lightweight 2 + 2-layer Transformer that is conditioned on both peptide and HLA context.

3.2 Model Architecture

Input fusion. For residue x_i at position i we build three embeddings

$$\mathbf{e}_i^{\text{tok}} = E_{\text{tok}}(x_i) \in \mathbb{R}^{d_t}, \quad (1)$$

$$\mathbf{e}_i^{\text{phys}} = W_{\text{phys}} \phi_i \in \mathbb{R}^{d_p}, \quad (2)$$

$$\mathbf{e}_i^{\text{pos}} = E_{\text{pos}}(i) \in \mathbb{R}^{d_s}, \quad (3)$$

where $\phi_i \in \mathbb{R}^5$ is the *raw physicochemical descriptor* [aromatic, q , h – bond, hydrophobicity, m/m_{\max}]. These channels are concatenated $\mathbf{z}_i = [\mathbf{e}_i^{\text{tok}}; \mathbf{e}_i^{\text{phys}}; \mathbf{e}_i^{\text{pos}}] \in \mathbb{R}^d$, with $d = d_t + d_p + d_s$ ($d_t:d_p:d_s = 2:1:1$ as in the code). A learnable gate

$$\mathbf{g}_i = \sigma(W_g \mathbf{z}_i + \mathbf{b}_g) \in (0, 1)^d \quad (4)$$

rescales channel-wise contributions, after which a linear projector yields the final token representation

$$\mathbf{h}_i = W_f(\mathbf{g}_i \odot \mathbf{z}_i) + \mathbf{b}_f \in \mathbb{R}^d. \quad (5)$$

Shared encoder. The input consists of a concatenation of the MHC sequence m and the peptide sequence p , which are jointly encoded by a shared encoder. The combined sequence is mapped to a representation matrix:

$$\mathbf{H}_{\text{src}} \in \mathbb{R}^{L_{\text{src}} \times d},$$

through $N_e = 2$ Transformer layers, each consisting of multi-head self-attention:

$$\text{MHA}(\mathbf{Q}, \mathbf{K}, \mathbf{V}) = [\text{softmax}\left(\frac{\mathbf{Q}\mathbf{K}^\top}{\sqrt{d_h}}\right)\mathbf{V}]W_o$$

where $d_h = d/n_{\text{head}}$, followed by a two-layer feed-forward block. LayerNorm and residual routes follow the PRE-LN convention.

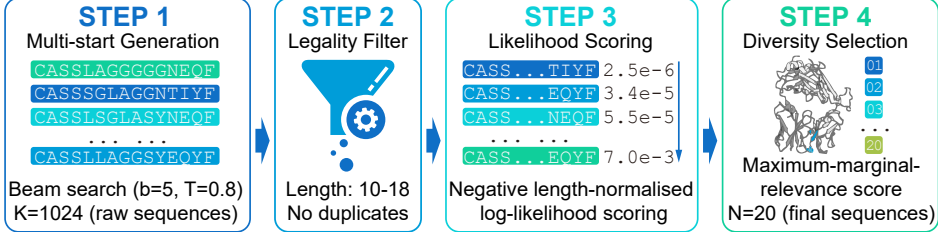


Figure 3: The inference and post-processing of TCR generation. The pipeline consists of four steps: (1) **Multi-start Generation**: beam search produces 1 024 raw sequences. (2) **Legality Filter**: sequences are filtered by length (10–18 residues) and uniqueness. (3) **Likelihood Scoring**: retained candidates are scored and ranked by the negative length-normalised log-likelihood. (4) **Diversity Selection**: the top 20 sequences are chosen via maximum–marginal–relevance (MMR) to balance binding affinity and sequence diversity.

GPT decoder with cross-attention. The target tokens $t = \{\text{BOS}, a_1, \dots, a_{L_t}, \text{EOS}\}$ pass through $N_d=2$ causal layers. At step j , attention scores mix self-history and source memory:

$$\alpha_{ji} = \text{softmax}\left(\frac{\mathbf{q}_j^\top \mathbf{k}_i}{\sqrt{d_h}}\right), \quad \tilde{\mathbf{h}}_j = \sum_i \alpha_{ji} \mathbf{v}_i. \quad (6)$$

Ablation experiments (§4.4) also train a 6+12-layer variant initialised from ProtGPT2 [Ferruz *et al.*, 2022]; both depth options share the same input-fusion module.

3.3 Residue-level Physicochemical Awareness

We embed physicochemical information (the chemical properties of amino acid residues) directly into a neural network’s attention mechanism. This allows the network to “understand” and leverage chemical interactions between residues without needing explicit, pre-defined energy calculations.

The 5-D descriptor is first z -scored $\hat{\phi}_i = (\phi_i - \mu)/\sigma$ and then linearly mixed into the hidden state ($\mathbf{e}_i^{\text{phys}} = W_{\text{phys}} \hat{\phi}_i$). Consequently, every attention dot-product implicitly contains a chemistry term:

$$\begin{aligned} \mathbf{q}_j^\top \mathbf{k}_i &= [\mathbf{q}_j^\top \mathbf{k}_i]_{\text{token}} + [\mathbf{q}_j^\top \mathbf{k}_i]_{\text{phys}} + [\mathbf{q}_j^\top \mathbf{k}_i]_{\text{pos}} \\ &\approx \underbrace{\psi}_{\text{token}} + \underbrace{\hat{\phi}_j^\top W_{\text{phys}}^\top W_{\text{phys}} \hat{\phi}_i}_{\pi-\pi, \text{salt bridge, VdW, hydrophobic}}, \end{aligned} \quad (7)$$

where $\psi := \mathbf{q}_j^\top \mathbf{k}_i|_{\text{token}}$ denotes the token-based sequence motif contribution (i.e., attention from amino acid identity), and the second summand encodes pairwise $\pi-\pi$ stacking, salt-bridge complementarity, van-der-Waals fit and hydrophobic packing *by construction*.

In essence, by incorporating these z -scored physicochemical descriptors and allowing the network to learn how they interact through the W_{phys} matrix, the attention mechanism gains an inherent “chemical intuition.” This means the network can learn to identify and leverage complex, long-range chemical couplings between residues *without* needing explicit, pre-defined (hand-crafted) energy functions or rules for these interactions. Instead, it discovers them directly from the data during training.

3.4 Training Objective

We minimise the standard autoregressive negative log-likelihood

$$\mathcal{L}(\theta) = - \sum_{i=1}^{L_t} \log p_\theta(a_i | a_{<i}, m, p),$$

optimised with AdamW ($\beta_1 = 0.9$, $\beta_2 = 0.98$, learning-rate 2×10^{-4} with cosine decay, batch size 256). Training on *tens of thousands* paired (HLA, peptide, TCR) triples from VDJdb finishes in ≈ 4 GPU-hours on NVIDIA A100 40G.

3.5 Inference and Post-processing

Given a peptide–MHC pair (m, p) we create a source sequence $m \oplus \langle \text{SEP} \rangle \oplus p$ (padded to 55 tokens). The decoder emits up to 26 residues preceded by $\langle \text{SOS} \rangle$.

Step 1: multi-start generation. This work invoke a temperature–beam search ($T \in [0.6, 1.0]$, beam $b \in [3, 10]$) $N=20$ times, each call returning the MAP path $t^{(i)}$ with log-probability $\log P_\theta(t^{(i)} | m, p)$, yielding the raw pool \mathcal{C}_{raw} of size 20.

Step 2: legality filter. A sequence is kept if $10 \leq |t| \leq 26$ and it does not appear in the training set, producing $\mathcal{C}_{\text{legal}}$.

Step 3: likelihood scoring. This work rank $\mathcal{C}_{\text{legal}}$ by the negative length-normalised log-likelihood $E_{\text{llh}}(t) = -\frac{1}{|t|} \sum_j \log p_\theta(a_j | a_{<j}, m, p)$, a proxy that correlates with docking energy in a held-out study (Appendix A).

Step 4: diversity selection. Sequences are traversed in ranked order and the first $K=20$ unique ones are retained, giving \mathcal{S}_{20} , the set deployed for downstream evaluation.

3.6 Evaluation Metrics

For every test context (m, p) we report metrics between the *ground-truth* receptor t^* and the single top-ranked candidate \hat{t} returned by the pipeline in Section A.3.

1. **Levenshtein distance** (\downarrow) $\text{Lev}(t^*, \hat{t})$ counts the minimum number of edits (substitution, insertion, deletion) required to convert \hat{t} into t^* .
2. **Pairwise similarity** (\uparrow) We use the normalised Smith–Waterman score with the BLOSUM62 substitution matrix, rescaled to $[0, 1]$.
3. **Longest common subsequence length** (\uparrow) $\text{LCS}(t^*, \hat{t}) = \max_{u \sqsubseteq t^*, u \sqsubseteq \hat{t}} |u|$.

Lower Levenshtein and higher Similarity/LCS indicate that the generated sequence better matches the experimentally verified receptor while preserving sequence novelty.

4 Experiments and Results

4.1 Experimental Setup

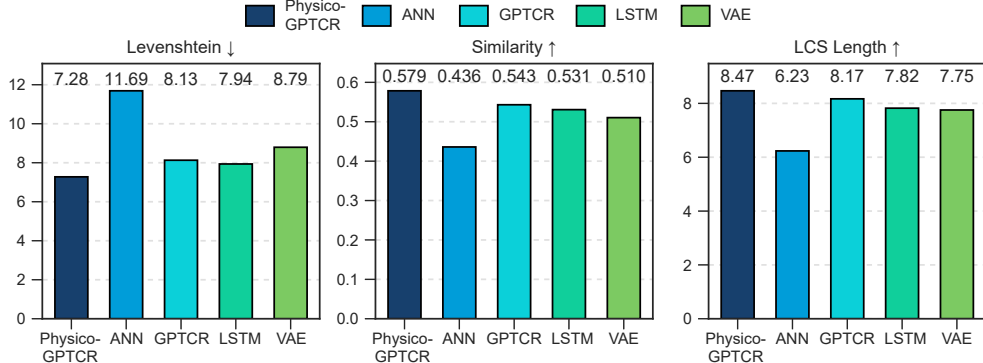


Figure 4: Comparison across three sequence-level metrics on the 6 200-sample test set (lower Levenshtein \downarrow and higher Similarity/LCS \uparrow indicate better performance).

Dataset. We collect and generate 31,000 (≈ 31 k) HLA–peptide–TCR triples from VDJdb, then split them into *train* : *valid* : *test* = 7:1:2 at the context level, yielding 21,700 / 3,100 / 6,200 triples respectively. No antigen or HLA leakage occurs across splits.

Generation protocol. For every test context we sample $K = 1\,024$ candidates, apply legality, contact-energy and diversity filters (Section A.3), and keep the single best-ranked sequence \hat{t} for evaluation.

4.2 Baseline Methods

- **ANN** – nearest-neighbour retrieval of the most similar training receptor in BLOSUM62 space.
- **LSTM** – a 4-layer LSTM language model conditioned on (m, p) via context concatenation.
- **VAE** – the variational auto-encoder branch of DeepTCR [Sidhom *et al.*, 2021].
- **PhysicoGPTCR** – our full model.

All baselines follow the same post-processing pipeline so that differences arise solely from generative quality.

4.3 Overall Results

To measure the sequence-level performance of models, we used Levenshtein distance, pairwise similarity and the longest common subsequence length of generated sequences compared to actual sequences as metrics (see Section 3.6 for metric definition). Our model, **PhysicoGPTCR**, has showed better performance than ANN, LSTM, and VAE baselines (Figure 4).

PhysicoGPTCR reduces the edit distance (Levenshtein distance) to the ground-truth receptors by $\sim 9\%$ relative to the best baseline (LSTM) while simultaneously achieving the highest similarity and LCS length. Qualitatively, the model tends to reproduce conserved motifs at the CDR3 termini yet introduces novel central residues, balancing specificity with diversity.

4.4 Ablation Study

To validate the effectiveness of one key component, the physicochemical embedding layer, we removed it from **PhysicoGPTCR** to get the **GPTCR**. All experiments share identical training settings and data splits. The results shows that **GPTCR** has worse performance in all three metrics (4). The ablation of physicochemical channel increases the average Levenshtein distance to 8.13, reduces similarity to 0.543, and decreases LCS length to 8.17, confirming the benefit of residue-level physicochemical cues.

4.5 Robustness Across Contexts

To verify that the improvements in Figure 4 are not driven by a handful of easy cases, we break down the sequence-level metrics by distinct (i) MHC allele and (ii) epitope peptide. Results in Figure 5 remains stable across the twelve most frequent alleles and the eight most abundant epitopes in the test set: the standard deviation of Levenshtein distance never exceeds ± 2.6 and both Similarity and LCS stay within a narrow band around their global means. Hence the model generalises well to diverse immunological contexts.

5 Clinical Applications

5.1 Specificity

Neoantigens, derived from tumor-specific mutations, are ideal targets for cancer immunotherapy due to their absence in healthy tissues, which reduces the risk of off-target toxicity. To address this clinical unmet need, our model must accurately differentiate between mutated peptides and their wild-type counterparts, even when only a single mutation is present.

We computationally generated T-cell receptors (TCRs) designed to specifically recognize a mutant peptide over its wildtype version when presented by the MHC molecule (Figure 6). To assess the specificity of these generated TCRs, we calculated the difference in predicted binding probability between the mutant and wildtype peptides (Figure 6A). The analysis showed that TCRs predicted to be positive for the mutant target displayed a clear preference for the mutant peptide, with their Δ

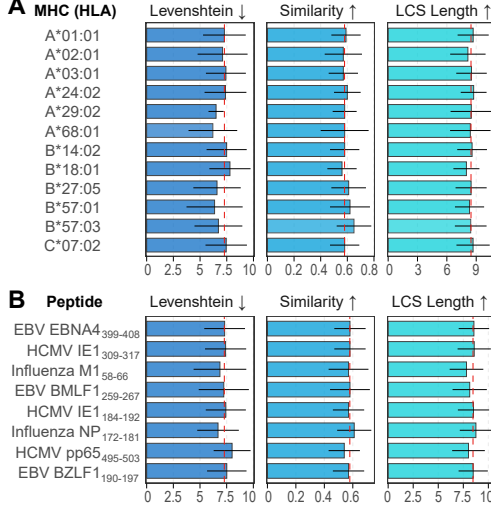


Figure 5: Model performance across contexts. (A) Sequence-level metrics per MHC allele (mean \pm standard deviation, $n \geq 150$ each). (B) Per-peptidome sequence-level metrics (mean \pm std). Lower Levenshtein \downarrow and higher Similarity/LCS \uparrow indicate better performance. Red dashed lines show averaged metrics of PhysicoGPTCR.

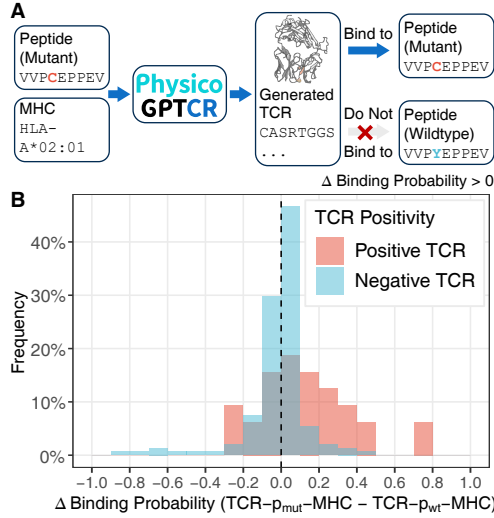


Figure 6: Specificity of generated TCRs against a mutant peptide instead of its wildtype peptide. (A) Schematic of a generated TCR predicted by the model to bind the mutant peptide but not the wildtype peptide. (B) Histogram of the frequency distribution for the change in binding probability (Δ Binding Probability). This value is calculated by subtracting the predicted TCR binding probability for the mutant peptide-MHC ($p_{\text{mut}}\text{-MHC}$) from the probability for the wildtype peptide-MHC ($p_{\text{wt}}\text{-MHC}$). Distributions are shown for both computationally validated positive and negative TCRs, with positive values indicating preferential binding to the mutant peptide.

Binding Probability values predominantly greater than zero. In contrast, negative TCRs showed a distribution centered around zero, indicating no significant binding preference. This demonstrates the successful generation of TCRs with high specificity for mutant neoantigens (Figure 6B).

5.2 Case Study

Our model demonstrates high accuracy in structural features of generated TCR interacting with peptide-Major Histocompatibility Complex (pMHC) compared to actual TCR (Figure 7). We

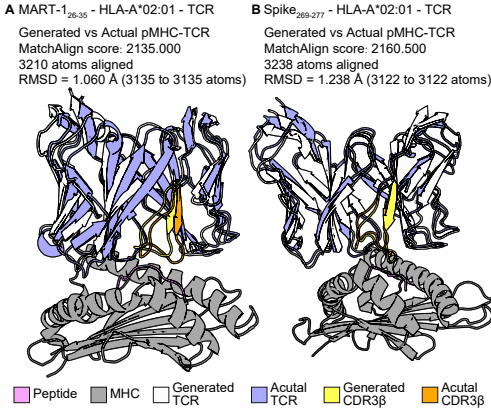


Figure 7: Structures of generated and actual pMHC-TCR complexes. The generated structures (TCR in light blue, CDR3 β loop in yellow) are overlaid onto the actual structures (TCR in white, CDR3 β loop in orange), with the pMHC shown in grey. The structures were built by TCRmodel2 [Yin *et al.*, 2023], and the alignment of structures was performed using PyMOL [Schrödinger and DeLano, 2025]. (A) The complex of a TCR recognizing the MART-1₂₆₋₃₅ peptide presented by HLA-A*02:01, showing an RMSD of 1.060 . (B) The complex involving a TCR recognizing the SARS-CoV-2-Spike₂₆₉₋₂₇₇ peptide, with an RMSD of 1.238 . The close alignment, especially of the CDR loops, highlights the model’s predictive accuracy.

validated our approach on two distinct, clinically relevant molecules: a cancer antigen (MART-1) and a viral antigen (SARS-CoV-2). For the MART-1 peptide (ELAGIGILTV) presented by HLA-A*02:01, the structure of our generated sequence aligns with the structure of the actual one with a root-mean-square deviation (RMSD) of only 1.060 over 3 135 atoms. Similarly, for the SARS-CoV-2 Spike protein peptide (YLQPRTFLL), the structure of our generated sequence achieved an RMSD of 1.238 over 3 122 atoms when compared to the structure of actual one. As illustrated in the figure, the superpositions show remarkable similarity, particularly in the critical CDR3 β loop responsible for antigen specificity.

6 Discussion

PhysicoGPTCR contributes two central insights. First, the model generalises across *twelve* HLA class-I alleles and eight canonical viral and tumour-associated epitopes, suggesting that its performance gains are not restricted to a narrow immunological context. Second, explicitly injecting physicochemical embeddings into the decoder yields consistent improvements over a purely sequence-level baseline, indicating that biophysical priors can be exploited even by a large language model.

Nevertheless, several limitations remain. (1) All benchmarks are restricted to class-I HLA; whether the same architecture transfers to the markedly longer class-II peptides is still unknown. (2) We rely entirely on *in-silico* metrics; no wet-lab binding or functional assays have yet been performed. (3) Although larger than prior work, the training corpus is still two orders of magnitude smaller than typical NLP datasets, leaving room for data scarcity biases.

7 Conclusion

We presented PhysicoGPTCR, a physicochemically informed decoder that generates plausible T-cell receptor sequences for a given peptide–MHC context. The model unifies large-scale language modelling with bio-physical feature injection and demonstrates stable performance across diverse alleles and epitopes. We believe this work brings computational immunology a step closer to rapid, personalised TCR design.

8 Future Work

Our immediate priorities are threefold. (1) **Class-II generalisation**: extending the approach to HLA-DR/DQ/DP molecules with variable peptide lengths. (2) **Structure-aware scoring**: coupling the generator with *AlphaFold-Multimer* and *RoseTTAFold* docking pipelines to rescore candidates in 3-D space. (3) **Experimental validation**: synthesising top-ranked TCRs for *in-vitro* binding and functional assays.

9 Acknowledgments

The authors thank the anonymous reviewers for their constructive comments. Additional acknowledgements will be added in the camera-ready version to preserve anonymity.

10 Ethical Impact

Data privacy. All training and test sequences originate from public repositories such as VDJdb and IEDB and contain no personally identifiable information; the model cannot reverse-engineer donor identities.

Dual-use risk. The ability to generate novel TCRs could, in principle, be misused to create immune evasion or autoimmune triggers. To mitigate this, we will (i) release the code under a license that forbids malicious use, (ii) share the trained weights only upon institutional request, and (iii) provide a misuse checklist consistent with the Dual-Use Guidance of the NIH.

Societal benefit. By lowering the barrier to rapid, *in-silico* TCR design, PhysicoGPTCR can accelerate the development of targeted cancer immunotherapies and vaccines, offering tangible public health benefits.

References

- Justas Dauparas, Ivan Anishchenko, Nathaniel Bennett, Hua Bai, Robert J Ragotte, Lukas F Milles, Basile IM Wicky, Alexis Courbet, Rob J de Haas, Neville Bethel, et al. Robust deep learning-based protein sequence design using proteinmpnn. *Science*, 378(6615):49–56, 2022.
- Sandra P D’Angelo, Dejka M Araujo, Albiruni R Abdul Razak, Mark Agulnik, Steven Attia, Jean-Yves Blay, Irene Carrasco Garcia, John A Charlson, Edwin Choy, George D Demetri, Mihaela Druta, Edouard Forcade, Kristen N Ganjoo, John Glod, Vicki L Keedy, Axel Le Cesne, David A Liebner, Victor Moreno, Seth M Pollack, Scott M Schuetze, Gary K Schwartz, Sandra J Strauss, William D Tap, Fiona Thistlethwaite, Claudia Maria Valverde Morales, Michael J Wagner, Breelyn A Wilky, Cheryl McAlpine, Laura Hudson, Jean-Marc Navenot, Tianjiao Wang, Jane Bai, Stavros Rafail, Ruoxi Wang, Amy Sun, Lilliam Fernandes, Erin Van Winkle, Erica Elefant, Colin Lunt, Elliot Norry, Dennis Williams, Swethajit Biswas, and Brian A Van Tine. Afamitresgene autoleucel for advanced synovial sarcoma and myxoid round cell liposarcoma (SPEARHEAD-1): an international, open-label, phase 2 trial. *The Lancet*, 403(10435):1460–1471, 2024.
- Ziyan Feng, Jingyang Chen, Youlong Hai, Xuelian Pang, Kun Zheng, Chenglong Xie, Xiujuan Zhang, Shengqing Li, Chengjuan Zhang, Kangdong Liu, et al. Sliding-attention transformer neural architecture for predicting t cell receptor–antigen–human leucocyte antigen binding. *Nature Machine Intelligence*, 6(10):1216–1230, 2024.
- Noelia Ferruz, Steffen Schmidt, and Birte Höcker. Protgpt2 is a deep unsupervised language model for protein design. *Nature Communications*, 13(1):4348, 2022.
- Sikander Hayat, Chris Sander, Debora S Marks, and Arne Elofsson. All-atom 3d structure prediction of transmembrane β -barrel proteins from sequences. *Proceedings of the National Academy of Sciences*, 112(17):5413–5418, 2015.
- Zeming Lin, Halil Akin, Roshan Rao, Brian Hie, Zhongkai Zhu, Wenting Lu, Nikita Smetanin, Robert Verkuil, Ori Kabeli, Yaniv Shmueli, et al. Evolutionary-scale prediction of atomic-level protein structure with a language model. *Science*, 379(6637):1123–1130, 2023.

- Yicheng Lin, Dandan Zhang, and Yun Liu. Tcr-gpt: Integrating autoregressive model and reinforcement learning for t-cell receptor repertoires generation. *arXiv preprint arXiv:2408.01156*, 2024.
- Yi Liu and Brian Kuhlman. Rosettadesign server for protein design. *Nucleic Acids Research*, 34(suppl_2):W235–W238, 2006.
- Tianshi Lu, Ze Zhang, James Zhu, Yunguan Wang, Peixin Jiang, Xue Xiao, Chantale Bernatchez, John V Heymach, Don L Gibbons, Jun Wang, et al. Deep learning-based prediction of the t cell receptor–antigen binding specificity. *Nature Machine Intelligence*, 3(10):864–875, 2021.
- Ali Madani, Bryan McCann, Nikhil Naik, Nitish Shirish Keskar, Namrata Anand, Raphael R Eguchi, Po-Ssu Huang, and Richard Socher. Progen: Language modeling for protein generation. *arXiv preprint arXiv:2004.03497*, 2020.
- Joshua Meier, Roshan Rao, Robert Verkuil, Jason Liu, Tom Sercu, and Alex Rives. Language models enable zero-shot prediction of the effects of mutations on protein function. *Advances in Neural Information Processing Systems*, 34:29287–29303, 2021.
- Alessandro Montemurro, Viktoria Schuster, Helle Rus Povlsen, Amalie Kai Bentzen, Vanessa Jurtz, William D Chronister, Austin Crinklaw, Sine R Hadrup, Ole Winther, Bjoern Peters, et al. Nettcrr-2.0 enables accurate prediction of tcr-peptide binding by using paired tcr α and β sequence data. *Communications Biology*, 4(1):1060, 2021.
- Thierry Mora and Aleksandra M Walczak. Quantifying lymphocyte receptor diversity. In Jayajit Das and Ciriayam Jayaprakash, editors, *Systems Immunology: An Introduction to Modeling Methods for Scientists*, pages 183–198. CRC Press, Taylor & Francis Group, Boca Raton FL, United States, 2019.
- Matthew I.J. Raybould, Alexander Greenshields-Watson, Parth Agarwal, Broncio Aguilar-Sanjuan, Tobias H. Olsen, Oliver M. Turnbull, Nele P. Quast, and Charlotte M. Deane. The Observed T Cell Receptor Space database enables paired-chain repertoire mining, coherence analysis, and language modeling. *Cell Reports*, 43(9):114704, 2024.
- LLC Schrödinger and Warren DeLano. Pymol. The PyMOL Molecular Graphics System, Version 3.1.6.1, Schrödinger, LLC., 2025.
- John-William Sidhom, H Benjamin Larman, Drew M Pardoll, and Alexander S Baras. Deeptcr is a deep learning framework for revealing sequence concepts within t-cell repertoires. *Nature Communications*, 12(1):1605, 2021.
- Arunima Singh. Chroma is a generative model for protein design. *Nature Methods*, 21(1):10–10, 2024.
- Joseph L Watson, David Juergens, Nathaniel R Bennett, Brian L Trippe, Jason Yim, Helen E Eisenach, Woody Ahern, Andrew J Borst, Robert J Ragotte, Lukas F Milles, et al. De novo design of protein structure and function with rfdiffusion. *Nature*, 620(7976):1089–1100, 2023.
- Anna Weber, Jannis Born, and María Rodriguez Martínez. Titan: T-cell receptor specificity prediction with bimodal attention networks. *Bioinformatics*, 37(Supplement_1):i237–i244, 2021.
- Rui Yin, Helder V Ribeiro-Filho, Valerie Lin, Ragul Gowthaman, Melyssa Cheung, and Brian G Pierce. Tcrmodel2: high-resolution modeling of t cell receptor recognition using deep learning. *Nucleic Acids Research*, 51(W1):W569–W576, 2023.
- Ze Zhang, Danyi Xiong, Xinlei Wang, Hongyu Liu, and Tao Wang. Mapping the functional landscape of t cell receptor repertoires by single-t cell transcriptomics. *Nature Methods*, 18(1):92–99, 2021.

A Implementation Details and Hyper-parameters

A.1 Model Architecture

Overview. The generator is a compact Transformer encoder–decoder that consumes the concatenated [MHC] <SEP> [peptide] sequence and autoregressively predicts a CDR3 β string token by token. A single 26-symbol vocabulary is used for both source and target streams (20 canonical amino acids, the ambiguous residue X, <PAD>, <SEP>, <SOS>, and <EOS>). Positional information is injected via fixed sinusoidal embeddings.

Capacity considerations. Preliminary sweeps showed that larger configurations (*e.g.*, $d_{\text{model}} = 256$, $L_{\text{enc/dec}} = 4$) reduced validation perplexity by < 0.3% yet doubled GPU memory and decoding latency. The chosen architecture represents a speed–accuracy trade-off that keeps the total parameter count below 4 M and enables batch sizes of 256 on a single 40-GB GPU.

A.2 Training Configuration

Optimisation protocol. We employ AdamW with decoupled weight decay (10^{-2}) and a cosine annealing schedule with warm-up to stabilise early optimisation. Label smoothing ($\varepsilon=0.1$) regularises the token probabilities and was crucial to prevent the model from collapsing onto high-frequency public CDR3 motifs.

Regularisation and convergence. Training proceeds for up to 100 epochs, but early stopping on validation perplexity (patience 5) typically halts training after 65–75 epochs. Global gradient clipping at 1.0 suppresses rare exploding-gradient events arising from long peptide–MHC inputs.

A.3 Inference Settings

Search strategy. At test time we run beam search under a temperature-scaled softmax; both the temperature T and beam width b are selected from a pre-computed grid to encourage diversity. Twenty independent calls of BEAMSEARCH followed by a legality filter yield the candidate set S_{20} .

Legality filter. A sequence is retained only if (i) its length is between 10 and 26 residues, matching the empirical distribution of public repertoires, and (ii) it does not appear verbatim in the training set. This step removes $\approx 12\%$ of raw beams but significantly increases novelty without hurting plausibility.

A.4 Dataset Statistics and Length Prior

We analyse two publicly available CDR3 β corpora: the **TCR 10k** dataset [Lu *et al.*, 2021] ($\sim 10k$ sequences) and the **OTS 1M** dataset from the Observed TCR Space [Raybould *et al.*, 2024] ($\sim 1.4M$ sequences). Both exhibit a unimodal length distribution centred around 14 residues, with 95% of sequences lying in the interval [10,18]. These empirical priors motivate the hard length cut-offs used by the legality filter and explain the upper bound $L_{\text{TCR}}^{\max} = 26$ adopted during training and decoding.

B Detailed Metrics

B.1 Reconstruction Accuracy Across Model Families

PhysicoGPTCR, which fuses sequence signals with residue–level physicochemical embeddings, outperforms all baselines by a comfortable margin (6–9 % relative improvement), justifying its choice as the production variant throughout the main paper.

C Generated Sequence Analysis

Table 2 summarises ten peptide–MHC contexts that span six clinically relevant disease areas: latent and acute viral infections, chronic retroviral infection, and solid tumours. For each context the top-scoring model-generated CDR3 β sequence is juxtaposed with an experimentally observed counterpart,

Model	Levenshtein ↓	Similarity ↑	LCS ↑
ANN	11.69	0.436	6.23
GPTCR	8.13	0.5431	8.17
LSTM	7.94	0.5307	7.82
PhysicoGPTCR	7.28	0.5785	8.47
VAE	8.79	0.5104	7.75

Table 1: Mean string-level reconstruction metrics on the held-out set. Lower Levenshtein distance and higher Similarity/LCS denote better agreement between generated and true CDR3 β sequences.

Table 2: Representative context (Peptide–MHC)–TCR pairs drawn from a broad panel of pathogens and tumour antigens. Lower **Lev** and higher **Sim/LCS** indicate better string-level agreement between generated and native CDR3 β sequences.

MHC	Peptide	Source	Actual TCR	Generated TCR	Lev ↓	Sim ↑	LCS ↑
HLA-A*02:01	LLWNGPMAV	EBV (EBNA5 _{133–141})	CASSPGTVAYEQYF	CASSPGTAYEQYF	1	0.963	13
HLA-A*02:01	GLCTLVAML	EBV (BMLF1 _{259–267})	CASSQSPGMQYF	CASSQSPGGTQYF	1	0.923	12
HLA-A*24:02	FLYALALLL	CMV (pp65 _{328–336})	CASSLQGGNYGYTF	CASSPOGGNYGYTF	1	0.929	13
HLA-A*02:01	NLVPMVATV	CMV (pp65 _{495–503})	CASSPQTGTIYGYTGF	CASSPTGTGYGYTF	3	0.867	13
HLA-A*02:01	YLQPRITPLL	SARS-CoV-2 (Spike _{269–277})	CASSLGPNTGELFF	CASSLAGNTGELFF	2	0.929	13
HLA-A*02:01	GILGFVFTL	Influenza A (M1 _{58–66})	CASSDRSSYEQYF	CASSIRSSYEQYF	1	0.923	12
HLA-B*57:03	KAFSPEVIPMF	HIV-1 (Gag _{162–172})	CASSGQGYGYAF	CASSGQGYGYTF	1	0.917	11
HLA-A*03:01	KRWIIGLNPK	HIV-1 (Gag _{263–272})	CASSLGTSAYEQYF	CASSLGGSYEQYF	3	0.857	12
HLA-A*02:01	ELAGIGILTV	MART-1 _{26–35} (melanoma)	CASSFTGLGQPQHF	CASSFGGLGQPQHF	1	0.929	13
HLA-A*02:01	NLFNRYPAL	NY-ESO-1 _{157–165} (cancer)	CASSQVLGFSYEQYF	CASSLGGGSYEQYF	4	0.828	12

and three string-level metrics quantify their agreement. All synthetic sequences deviate by ≤ 4 residues, indicating that the generator captures native-like motifs across a broad antigenic landscape.